Open access • Journal Article • DOI:10.1088/1361-6463/AA562C

Routes to increase the conversion and the energy efficiency in the splitting of CO2 by a dielectric barrier discharge — Source link

Alp Ozkan, Alp Ozkan, Annemie Bogaerts, François Reniers

Institutions: Université libre de Bruxelles, University of Antwerp

Published on: 30 Jan 2017 - Journal of Physics D (IOP Publishing)

Topics: Dielectric barrier discharge, Plasma parameters, Dielectric, Plasma and Atmospheric pressure

Routes to increase the conversion and the energy efficiency in the splitting of CO_2 by a dielectric barrier discharge

Routes to increase the conversion and the energy efficiency in the splitting of CO_2 by a dielectric barrier discharge

A. Ozkan[1,2], A. Bogaerts[2], F. Reniers[1]

[1] Université Libre de Bruxelles, Chimie analytique et chimie des interfaces (CHANI), Campus de la Plaine, CP255, boulevard du Triomphe, 1050 Bruxelles, Belgium

[2] Universiteit Antwerpen, Research group PLASMANT, Universiteitsplein 1, 2610 Antwerpen-Wilrijk, Belgium

Abstract

We present here routes to increase the CO_2 conversion into CO using an atmospheric pressure dielectric barrier discharge. The change in conversion as a function of simple plasma parameters, such as power, flow rate, but also frequency, on-and-off pulse of the power, thickness and chemical nature of the dielectric, wall and gas temperature, is described. By means of an in-depth electrical characterization of the discharge (effective plasma voltage, dielectric voltage, plasma current, number and lifetime of the microdischarges), combined with infrared analysis of the walls of the reactor, optical emission spectroscopy for the gas temperature, and mass spectrometry for the CO_2 conversion, we propose a global interpretation for the effect of all the experimental parameters on the conversion and efficiency of the reaction.

Introduction

The conversion of CO_2 into CO using plasma has been the subject of numerous studies these last years. Indeed, after having been considered as a waste for decades, its increase in the atmosphere, leading to the currently observed global warming, progressively lead the scientific community to focus on this molecule. Reduction of the CO_2 emission and CO_2 storage are well known routes, but more recently there is increasing interest in the cradle to cradle approach, which tends at considering CO_2 not anymore as an end-product waste of many chemical reactions, but as a reactant for a new chemistry. Together with that approach, the global need for new energy routes, and thus the development of renewable energies, lead the scientific community to imagine storing excess-electricity into chemical molecules, such as carbon monoxide, or methanol. For that purpose, and despite its very high stability, CO_2 could become a useful reactant. Similarly, CO can be seen as the first building block for organic chemistry.

Several routes have been proposed already, involving low or reduced pressure microwave plasma [1-4], atmospheric pressure gliding arc [5-8] or dielectric barrier discharge (DBD) plasma [9-17]. The use of ns-pulse [18] or spark [19-23] discharges has also been developed. A wide variety of information has been published, and the main parameters that might influence the CO_2 conversion are now more or less understood. In separate papers, we have extensively studied some of these individual effects

on the conversion in an atmospheric pressure DBD [15, 24, 25]. The aim of this paper is to summarize and integrate the effect of these parameters, in an attempt to explain them, and to draw a general route aiming at increasing the conversion and energy efficiency of the CO_2 splitting in a DBD.

The CO_2 splitting reaction considered here is:

$$CO_2(g) \rightarrow \frac{1}{2}O_2(g) + CO(g)$$

This reaction is highly endothermic and endergonic ($\Delta H^0 = 283\ \mathrm{kJ \cdot mol^{-1}}$, $\Delta G^0 = 257\ \mathrm{kJ \cdot mol^{-1}}$).

Experimental details

The experiments have been carried out in a cylindrical DBD reactor previously described [15, 24, 25]. The key aspect of our approach is the combination of various analytical techniques used to characterize the plasma and the CO_2 conversion, which can be summarized by Figure 1.

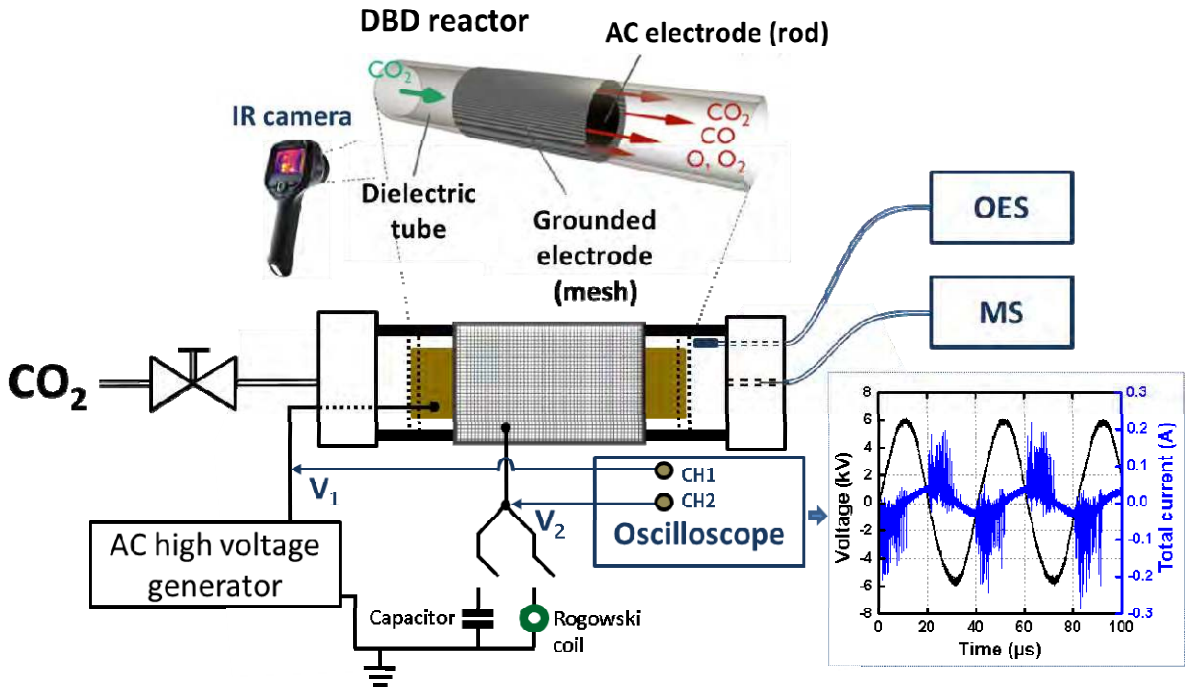

Figure 1: Scheme of the experimental setup and the DBD plasma reactor (gap = 2 mm; dielectric thickness = 2 mm; length of the discharge zone = 100 mm). A typical AC voltage-current waveform is also shown at the bottom right of this figure.

The CO_2 conversion and the energy efficiency of the CO_2 dissociation process are analyzed by the evolution of the intensity of the *m/z* peak at 44 recorded by an atmospheric mass spectrometer (Hiden analytical QGA) with a 70 eV electron energy fixed in the ionization chamber.

The equations to determine the conversion of CO_2 and the energy efficiency are given in Table 1.

Table 1: Formulas for conversion, energy efficiency, energy density and specific energy input.

Parameter	Formula	#
Conversion	$\chi_{CO_2\,(\%)} = \frac{I_{CO_2}^{plasma\ OFF} - I_{CO_2}^{plasma\ ON}}{I_{CO_2}^{plasma\ OFF}} \times 100\%$	Eq. 1
Energy efficiency	$\eta_{CO_2\,(\%)} = \chi_{CO_2\,(\%)} \cdot \frac{\Delta H^0_{298K\ (eV.molecule^{-1})}}{SEI_{(eV.molecule^{-1})}}$	Eq. 2
Energy density	$E_{d\,(J.cm^{-3})} = \frac{Absorbed\ power_{(J.s^{-1})}}{Gas\ flow\ rate_{(cm^3.s^{-1})}}$	Eq. 3
Specific energy input	$SEI_{(eV.molecule^{-1})} = \frac{E_{d\,(J.cm^{-3})} \times 6.24x10^{18}{}_{(eV.J^{-1})} \times 24500_{(cm^3.mol^{-1})}}{6.022x10^{23}{}_{(molecule.mol^{-1})}}$	Eq. 4

Where I_{CO2} is the intensity of the mass spectrometry signal of CO_2 at *m/z* = 44. The absorbed power is determined by the Lissajous method.

All the electrical measurements are performed using a two-channel digital oscilloscope (Tektronix DPO 3032). The applied voltage (V_1) is measured with a high voltage probe (Tektronix P6015A) while the DBD voltage supplied by the generator (V_{DBD}) is determined by subtracting V_2 from V_1, as represented in Figure 1. The potential V_2 is measured either through a capacitor of 10 nF or a Pearson 2877 Rogowski coil current probe, both placed in series with the DBD.

V_{DBD} is also expressed as the sum of two voltages: the dielectric voltage (V_{diel}) and the effective plasma voltage ($V_{pl,eff}$). In filamentary mode such as in a CO_2 discharge, the plasma voltage is considered as the effective voltage, since the filamentary mode is responsible for an inhomogeneous electric field in the whole electrode-barrier gap, which is different from the case of a diffuse and homogeneous glow discharge [26-29]. Therefore, $V_{pl,eff}$ should be considered as an average value and represents typically 70-80% of the V_{DBD} [15].

DBDs can be represented by an equivalent electrical circuit, before and during a plasma ignition. It consists of two capacitors in a serial connection: one for the gap with gas and the other one for the dielectric barrier(s). A variable resistor which represents the microdischarge channel can be included.

The equations to extract the effective plasma voltage are presented hereunder.

$$V_{DBD}\,(t) = V_{pl,eff}\,(t) + V_{diel}\,(t) \qquad \text{Eq. 5}$$

The current in dielectric capacitor can be described mathematically as follows:

$$i_{diel}(t) = i_{DBD}(t) = C_{diel}\frac{dV_{diel}(t)}{dt} \qquad \text{Eq. 6}$$

In order to determine the voltage components, the dielectric voltage is obtained by integrating equation 2 as follows:

$$V_{diel}(t) = \frac{1}{C_{diel}}\int_0^t i_{DBD}(\tau)d\tau + V_{diel}(0) \qquad \text{Eq. 7}$$

And the gap voltage can be obtained by substituting equation 7 into equation 5.

$$V_{pl,eff}(t) = V_{DBD}(t) - \frac{1}{C_{diel}} \int i_{DBD}(\tau) d\tau - V_{diel}(0) \qquad \text{Eq. 8}$$

V_{diel} *(0)* corresponds to the memory voltage that is a consequence of the charge accumulated in the previous half period.

The external capacitor of 10 nF allows to evaluate its electrical charge $Q_{pl}(t)$ and therefore the discharge power, or absorbed power (P_{abs}) by the plasma, via the Lissajous method [30-37]. This absorbed power divided by the gas flow rate is the *SEI* (specific energy input).

The total current of the discharge (i_{DBD}), as shown in the typical AC voltage-current waveform inserted in Figure 1, is recorded using a Rogowski coil which, contrarily to a resistance, can respond to fast changing currents thanks to its low inductance (rise time of 2 ns and drop rate of 0.2%/µs). The total current is the sum of the plasma or discharge current (i.e. conduction current) and the dielectric current (i.e. capacitive current). Several current short peaks, present at each half period, represent the active current i_{pl}. On the other hand, the displacement current is seen as the sinusoidal trend of the current profile. It can be directly determined on the oscillogram by fitting a sinusoidal function to the signal. By subtracting the displacement current from the total current, the active current can be calculated. The gas temperature is obtained from optical emission spectroscopy (OES). The OES measurements are performed with an Andor Shamrock-500i spectrometer (0.500 meter focal length, triple grating imaging) including an Andor DU420A-OE CCD camera. The light emitted by the discharge in the gap is collected by an optical fiber and transmitted to the entrance slit (50 µm) of the monochromator. The optical fiber is thus placed at the exit of the reactor in parallel to the reactor and pointing to the gap. There, the light is collimated, diffracted, focused on the exit slit and finally captured by the CCD camera. Each optical emission spectrum is acquired with either the 1800 grooves/mm or the 2400 grooves/mm grating (blazed at 500 nm and 250 nm). The reactor wall temperature is recorded with a FLIR E40 infrared camera with a resolution of 160x120 pixels and a thermal sensitivity lower than 0.07°C at 30°C. The FLIR ResearchIR software is used to control, record and analyze the temperature profiles in a range from -20°C to +650°C. The emissivity coefficients of the different materials are introduced in the software. The temperature is calibrated at room temperature.

Results, routes and discussion

Decreasing the flow rate increases the conversion, but it lowers the energy efficiency.

Figure 2a shows the effect of flow rate on the conversion of CO_2 and its energy efficiency. High conversion can be achieved at low flow rates. This has also been shown by others, e.g., [32]. The generally accepted explanation is that reducing the flow rates means increasing the residence time, leading to a higher probability of interaction between the electrons and the CO_2 molecules, and therefore more conversion. Moreover, decreasing the flow rate leads to an increase of the plasma voltage ($V_{pl,eff}$) as can be seen in Figure 2b. A higher plasma voltage means that the electrons responsible for CO_2 dissociation are more accelerated since the electric field is stronger. The electron temperature is therefore higher. This combination of a longer residence time and higher plasma voltage at low flow rates explains the higher conversion of CO_2. However, this conclusion is not very convenient for further industrial applications where usually high flow rates are required. Moreover,

the corresponding energy efficiency is low at these conditions, which is like expected from the definition (see Table 1 above). The lowest flow rate investigated here, i.e., 50 $mL_n.min^{-1}$, yields a CO_2 conversion of almost 35%, combined with an energy efficiency of 6%, which is in the same order or somewhat higher even, than typical results presented in literature for a DBD [32].

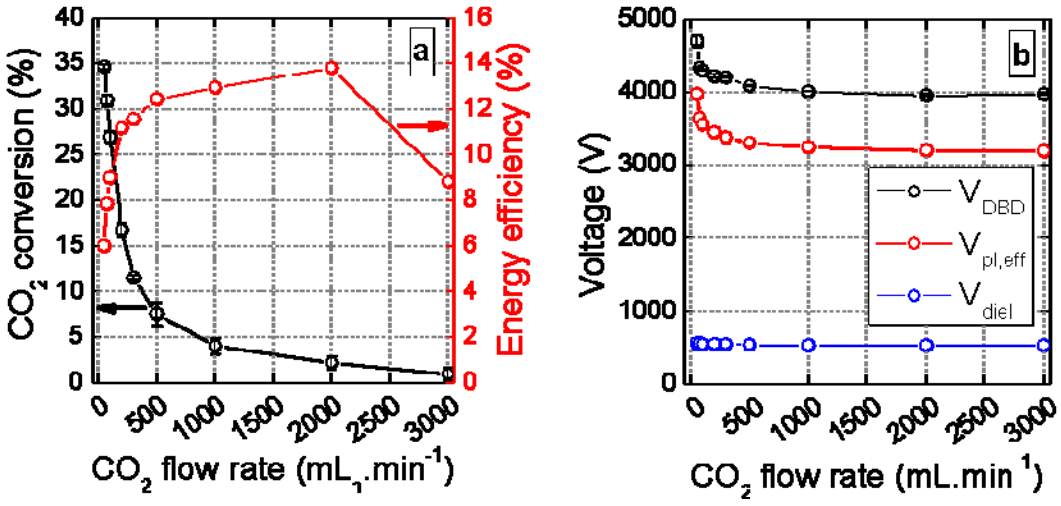

Figure 2: (a) CO_2 conversion and energy efficiency of the CO_2 splitting process; (b) voltage components versus the CO_2 flow rate at a fixed power and frequency (P_{abs} = 50-55 W according to the flow rate, f = 28.6 kHz)

Decreasing the frequency leads to an increase in the conversion and energy efficiency

Figure 3 shows the evolution of the CO_2 conversion and the energy efficiency with increasing frequency.

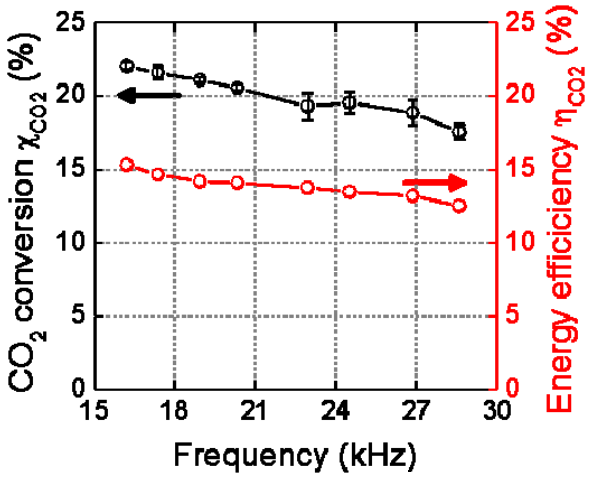

Figure 3: CO_2 conversion and energy efficiency as a function of the frequency, P_{abs} = 55 W, $\Phi(CO_2)$ = 200 $mL_n.min^{-1}$.

Although experiments were performed in a limited frequency range (15-30 kHz), some effect is still visible in the CO_2 conversion, as well as in the energy efficiency, which both slightly decrease with

increasing frequency. Figure 4 shows that, although the number of microdischarges (N_{md}) decreases per half period when the frequency increases, because of the shorter periods upon the increasing frequency, the total number of microfilaments for the same time unit (120 µs) remains constant. Similarly, the mean lifetime of the microdischarges (L_{md}) is unchanged in this frequency range. Hence, the microdischarges cannot explain the effect of frequency. The discharge current (i_{pl}, which is calculated from the accumulated plasma charge Q_{pl}) seems to slightly increase with frequency, so this can also not explain the drop in CO_2 conversion and energy efficiency upon rising frequency.

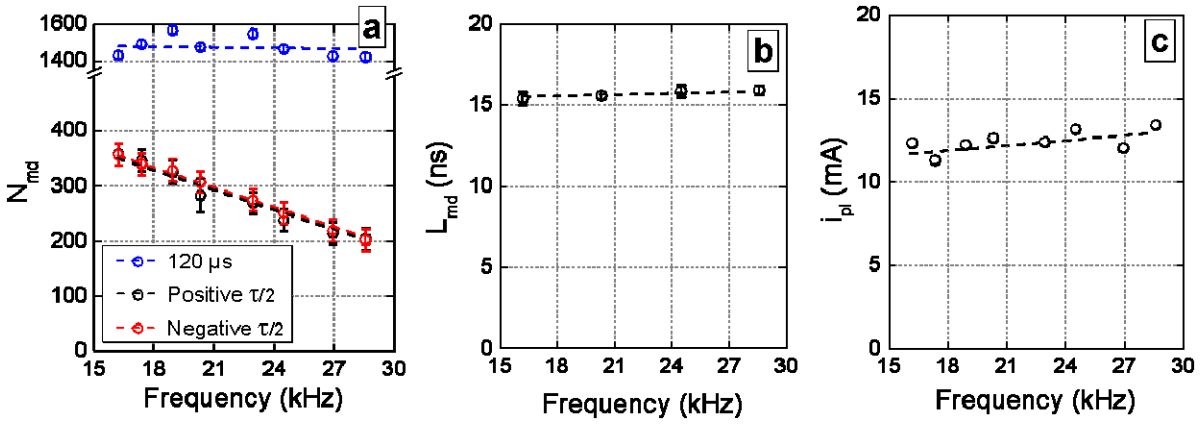

Figure 4: (a) Number and (b) lifetime of the microdischarges per half period (τ/2) and for τ_{anal} = 120 µs and (c) conduction current, as a function of the frequency, P_{abs} = 55 W, $\Phi(CO_2)$ = 200 $mL_n.min^{-1}$.

However, Figure 5 shows that, for a constant power (55 W absorbed power), the plasma voltage decreases with increasing frequency. Therefore, the drop in CO_2 conversion can be attributed to a decrease of the electric field inside the plasma discharge. Because of that, the average energy of the electrons is lowered and therefore, less electrons are able to participate in the CO_2 dissociation process. The reason for the drop in voltage has been already studied in detail for example by Valdivia-Barrientos et al. [38]. They showed that a DBD presents a higher memory voltage formation by charge accumulation on the dielectric surface when operating at higher frequency. The resulting breakdown voltage is thus lowered upon increasing operating frequency (valid in the range of kHz). In fact, the sustaining voltage present during the plasma ignition is lower than the ignition voltage at the very beginning of the discharge process. This is due to the polarization of the dielectric surface, always present when the polarity of the voltage is reversed [39].

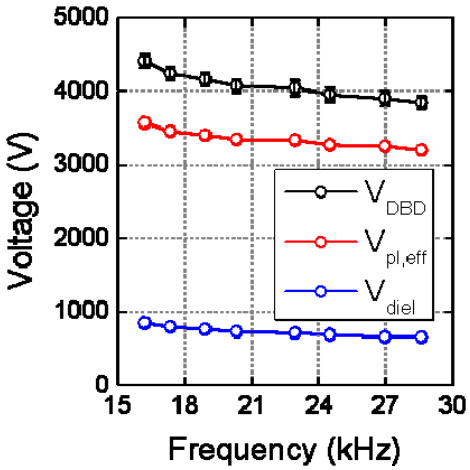

Figure 5: Applied voltage (V_{DBD}), plasma voltage ($V_{pl,eff}$) and voltage over the dielectric (V_{diel}) as a function of frequency at P_{abs} = 55 W, $\Phi(CO_2)$ = 200 $mL_n.min^{-1}$.

Increasing the plasma power increases the conversion, and only slightly lowers the energy efficiency

Figure 6 shows that the CO_2 conversion rises linearly with power, reaching a value as high as 28% at 100 W and a flow rate of 200 $mL_n.min^{-1}$. In the same power range, a slight decrease in the energy efficiency is measured from 12.5% to 11%. These trends are logical, because more energy is put into the system, leading to a higher electron density [40, 41], and to more CO_2 conversion. At the same time, as the rise in CO_2 conversion is less pronounced than the rise in *SEI*, the energy efficiency drops slightly with increasing power, as predicted by equation 2.

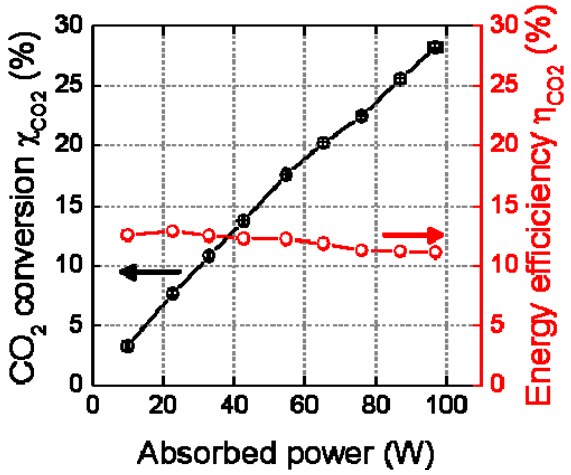

Figure 6: CO_2 conversion and energy efficiency as a function of the absorbed power, for f = 28.6 kHz, and $\Phi(CO_2)$ = 200 $mL_n.min^{-1}$.

Increasing the dielectric thickness increases the conversion and energy efficiency.

Figure 7 shows the CO_2 conversion and energy efficiency with increasing dielectric thickness, for absorbed powers varying from 10 to 70 W. A thicker dielectric leads to a higher conversion and energy efficiency.

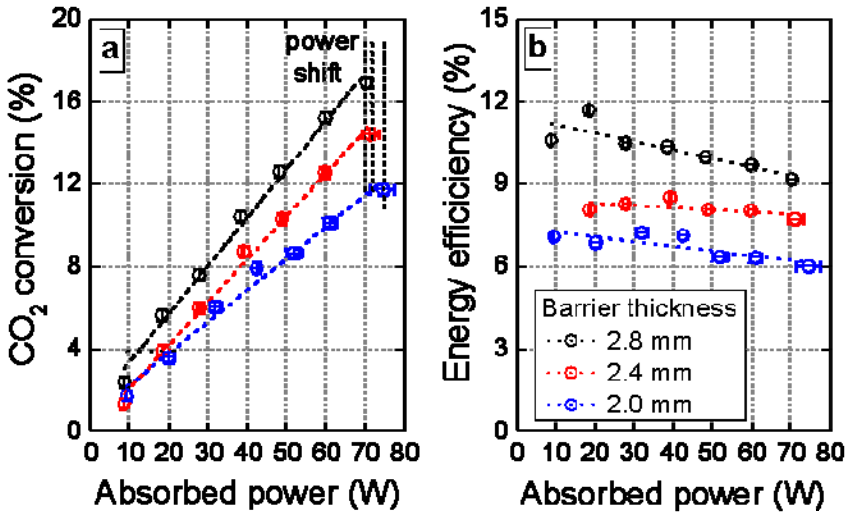

Figure 7: (a) CO_2 conversion and (b) energy efficiency as a function of the absorbed (plasma) power for three different dielectric thicknesses of pyrex (2.0, 2.4 and 2.8 mm); f = 28.6 kHz; $\Phi(CO_2)$ = 200 $mL_n.min^{-1}$.

As shown above when discussing the effect of the power, the absorbed power increases with the voltage applied to the DBD reactor. At fixed power of 60 W, Figure 8 illustrates that V_{DBD} can significantly rise with the dielectric thickness, increasing linearly from 5050 V to 5600 V (RMS values) for a barrier thickness ranging from 2.0 to 2.8 mm. As V_{DBD} is the sum of the averaged plasma voltage ($V_{pl,eff}$) and the dielectric voltage (V_{diel}), it is obvious from Figure 8 that the rise in V_{DBD} is attributed to V_{diel}, while the plasma voltage remains constant, close to 3800 V. As $V_{pl,eff}$ remains constant, so does the electric field. This parameter can therefore not explain the rise in CO_2 conversion. However, through a detailed analysis of the currents, one can extract information about the microdischarges, i.e. their individual features such as their average lifetime and electrical charge, but also their collective features such as the plasma charge accumulation and their total number (N_{md}) for a given analysis time (e.g. period of applied voltage, or residence time). Increasing the barrier from 2.0 to 2.8 mm leads to a significant increase of N_{md} (from 465 to 506), as is visible on the pictures of Figure 9. This increase in N_{md} appears to be of great importance for the CO_2 conversion despite the fact that the mean lifetime of the microdischarges slightly decreases upon an increasing barrier thickness. As the reactor volume is the same, independent of the barrier thickness, the probability for a single CO_2 molecule to pass through the discharge and interact with at least one microdischarge therefore increases for the thicker barriers. As a result, a higher CO_2 conversion (and thus energy efficiency, because power and flow rate are constant) is obtained.

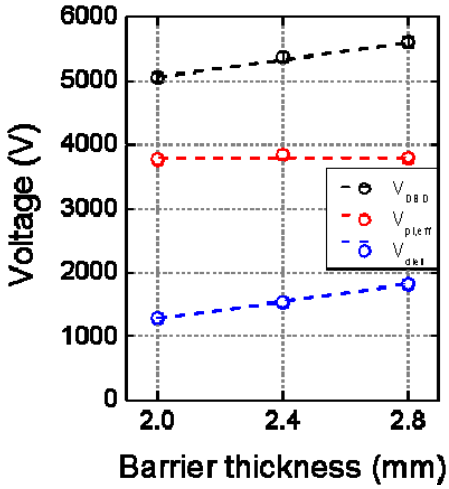

Figure 8: Voltage components as a function of the dielectric thickness at a given absorbed power P_{abs} = 60 W; f = 28.6 kHz; $\Phi(CO_2)$ = 200 $mL_n.min^{-1}$.

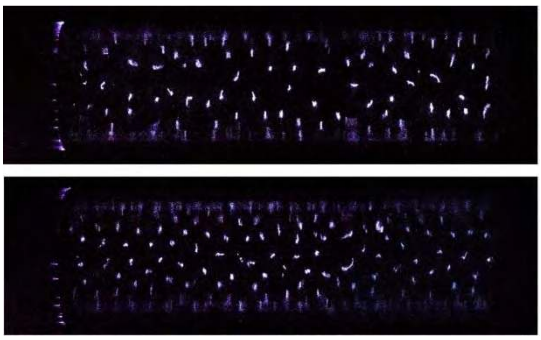

Figure 9: Pictures of the microdischarges observed through the pyrex and the outer mesh electrode, at same power, frequency and flow rate (for a camera aperture of 1/100 s). The barrier thickness is (top) 2.0 mm, (bottom) 2.8 mm. The number of microdischarges counted per one period, with the electrical characterization method described in [24], is equal to 465 for the 2.0 mm barrier, and 506 for the 2.8 mm barrier thickness.

The nature of the dielectric has a complex influence on the conversion.

Changing the nature of the dielectric material may lead to various electrical changes in the discharge. Indeed, while there is a simple trend when increase the dielectric thickness, changing the nature of the dielectric changes many physical parameters, such as the electrical permittivity, the thermal conductivity (Table 2), the capacitance, and the surface roughness (not speaking about a possible surface chemistry effect). We performed experiments using 2 mm thick Alumina, Mullite, Pyrex and Quartz dielectric barriers. Somewhat higher conversion and energy efficiencies are obtained for alumina and quartz, as can be seen in Figure 10.

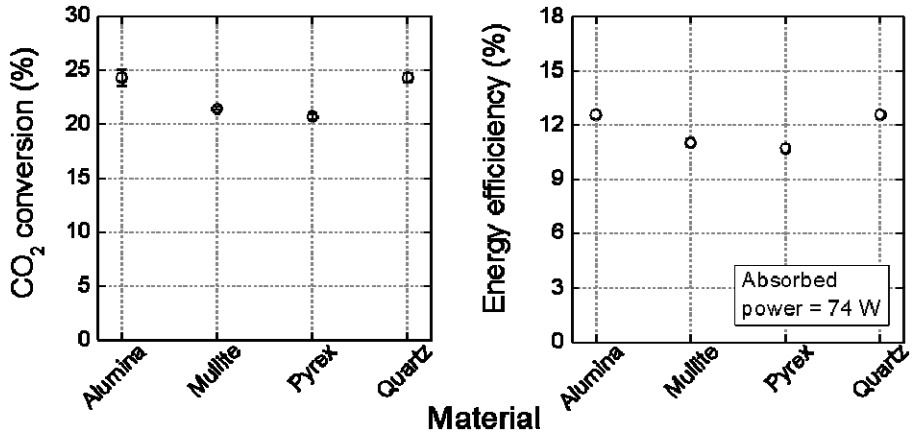

Figure 10: CO_2 conversion (left graph) and energy efficiency (right graph) for four different dielectric materials; P_{abs} = 74 W; f = 27.1 kHz; $\Phi(CO_2)$ = 200 $mL_n.min^{-1}$.

An electrical investigation of the plasma reveals that quartz allows delivering the highest voltage in the plasma (see Table 2). This leads to higher energy electrons, and therefore to a higher conversion. Similarly, quartz has the highest dielectric voltage, together with Pyrex, which leads to a higher number of microdischarges. As discussed above, the latter favors the probability of reaction between high energy electrons and the CO_2 molecules, and thus it favors the conversion. The same electrical characterization shows that the plasma current is the highest with the alumina dielectric. Moreover,

the high roughness of alumina favors the formation of microdischarges (see Table 2). These two parameters together can explain the better conversion with alumina.

Table 2: Relative permittivity, thermal conductivity, roughness of the dielectric surface (* obtained via profilometry), applied voltage, plasma voltage, dielectric voltage, plasma current, number of microdischarges per period and mean lifetime of the microdischarges for the four dielectric materials at a fixed absorbed power (P_{abs} = 74 W), a fixed frequency (f = 27.1 kHz) and a fixed gas flow rate ($\Phi(CO_2)$ = 200 $mL_n.min^{-1}$).

		Alumina	Mullite	Pyrex	Quartz
Relative permittivity (ε_r)		9.6	6.0	4.6	3.8
Thermal conductivity ($W.m^{-1}.K^{-1}$) (at 20°C)		29	2	1.1	1.4
Roughness of the dielectric surface R_{RMS} (nm)*		6800	3100	780	89
Voltage (V)	V_{DBD}	4389 ± 61	4831 ± 50	5170 ± 36	5735 ± 93
	$V_{pl,eff}$	3633	3814	3662	4242
	V_{diel}	756	1017	1508	1494
Plasma current (mA)	i_{pl}	15.6 ± 0.3	10.5 ± 0.4	9.9 ± 0.1	11.2 ± 0.5
Number of microdischarges (-)	N_{md}	556 ± 13	436 ± 11	442 ± 2	476 ± 16
Mean lifetime of microdischarges (ns)	L_{md}	14.8 ± 0.4	13.1 ± 0.3	13.2 ± 0.3	12.5 ± 0.3

The wall temperature and the gas temperature should remain as cold as possible

As a matter of fact, every part of the energy which contributes to the heating of the gas is considered as lost for the conversion of CO_2. Indeed, contrary to the CO_2 splitting by microwave plasma, which involves routes through vibrational excitation [42-45], the splitting of CO_2 in a DBD is supposed to proceed through electronic excitation/dissociation [42, 45, 46]. Moreover, a heated gas induces a thermal expansion, which leads to a decrease of the residence time in the reactor. In order to avoid excessive heating of the gas, the material of the wall of the reactor, and the thickness of the dielectric should be selected to have a high thermal conductivity (see Table 2 and Figure 11). This can also partly explain why alumina performs well as dielectric barrier material. Furthermore, switching off the power at high frequency, such as described in the next part of this paper, also contributes to cool down the system. Finally, a cooling system can also be placed in contact with the reactor.

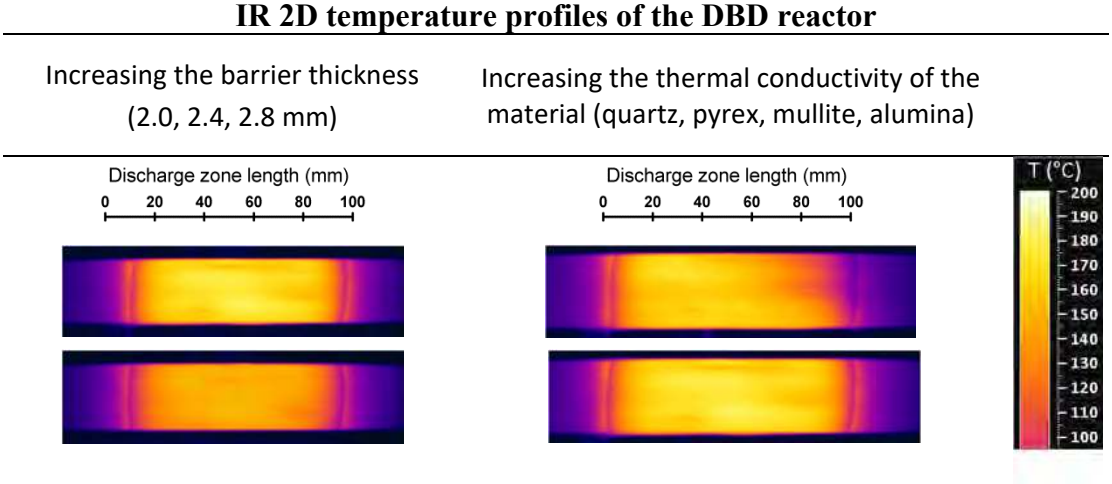

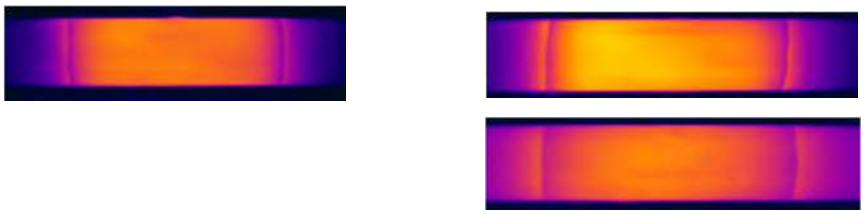

(a) (b)

Figure 11: 2D temperature profiles of the DBD reactors for (a) 2.0, 2.4 and 2.8 thick pyrex (top to bottom) and (b) from top to bottom 2.00 mm thick quartz, pyrex, mullite, alumina, for P_{abs} = 75 W, process time = 4 min. The black graded line indicates the length of the outer electrode, i.e. the discharge region.

As shown in Figure 11a, the heat dissipation is much higher in thicker dielectric materials, yielding a lower wall temperature in case of the 2.8 mm thickness of the barrier. The average temperature of the mesh outer electrode is 169, 151 and 134°C for the dielectric barrier thickness of 2.0, 2.4 and 2.8 mm, respectively. Moreover, the wall temperature outside of the discharge zone is also getting lower from 51 to 46°C when increasing the barrier thickness. Thus, the heat appears more confined in the discharge region for the thinner dielectric.

In Figure 11b, the average temperature of the mesh outer electrode is 136°C in case of alumina, against 149°C, 157°C and 169°C in case of mullite, quartz and pyrex, respectively. Moreover, the wall temperature outside of the discharge zone is quite elevated for alumina (almost 80°C) while it is only 45°C for the three other materials. Thus in the latter cases, the heating appears clearly confined in the discharge region. The different surface temperature might also yield a different gas temperature, and this may also affect the CO_2 conversion.

Pulsing the power increases the conversion and energy efficiency

Instead of injecting the power in a continuous AC mode, one can inject the same total power but in condensed time by switching the generator ON and OFF at a high frequency. This pulsed mode (sometimes called burst mode) is represented schematically in Figure 12. For an applied power of 50 W, when the duty cycle is 50%, meaning the plasma is “off” and “on” 50% of the time, the effective power during the “on” time is therefore 100 W. The CO_2 conversion increases from 16% for a continuous AC plasma to 26% for a 50% burst plasma, as is clear from Figure 13. Similarly, the energy efficiency increases from 15% to 23%. This increase in conversion can mainly be attributed to the strong increase of the DBD voltage. By changing this parameter, there is no significant change in the dielectric voltage, so the increase in V_{DBD} leads to an increase in the effective plasma voltage. For instance, for an applied power of 50 W, V_{DBD} is 3900 V for a pure continuous AC plasma, and 4300 V for a 50% burst mode (for a process time of 150 s). This higher voltage induces a higher electric field, and therefore a higher electron temperature, which increases the CO_2 conversion. A side effect of the fact that the plasma is switched on and off is a decrease of the gas temperature in the burst mode compared to the continuous mode. Thus, the gas in the discharge zone has time to cool down. Depending on the OES probe used (i.e., the FPS of N_2 or the Angstrom CO band; see details in [25]), the temperature drops from 610 to 563 K or from 530 to 455 K when going from a pure continuous plasma to a 50% burst plasma. Thus, there is more energy lost in thermal heating in a continuous plasma.

Moreover, the microdischarges are more spread out in the discharge zone in the case of a burst regime, as can be deduced from Figure 14, although the number of microdischarges is slightly higher instantaneously in the case of pure AC regime (400 N_{md}/τ for a D_{cycle} = 100% and 340 N_{md}/τ for a D_{cycle} = 50%, determined by electrical characterization). The repartition of the microdischarges is enhanced in a microsecond timescale, which is much smaller than the timescale of the reactive gas (CO_2) travelling the discharge zone, as the residence time of the gas is about 4.5 s for a gas flow rate of 200 $mL_n.min^{-1}$ (the volume and the length of the discharge zone are 15.1 cm^3 and 100 mm, respectively). The reason of this better repartition of microdischarges throughout the discharge zone arises from the fact that there is no memory effect in the case of the burst regime. Indeed, this effect, which is described as the localization of filaments in space and in time, is only present in the case of the pure classical AC regime and it can be explained in terms of volume mechanisms, or more importantly in terms of charge accumulation on the dielectrics [39]. The filaments have the tendency to always light up at the same location in the pure AC regime [47, 48]. There are more "intense" filaments, located at the same position, in the continuous mode, whereas in the burst mode (for lower duty cycles), the less intense filaments can light up everywhere, as there is no memory effect (or less pronounced in contrast to the pure AC mode), taking into consideration the fact that the high-voltage is repeatedly switched off. As a consequence, the CO_2 molecules, whose travel time in the reactor is around 4.5 s, have more chances to encounter filaments, which form the basis of the plasma reactivity, in the burst mode. Giving the fact that the electric field is higher and the fact that the microdischarges have a better repartition throughout the gap in the burst mode, the conversion and energy efficiency are enhanced.

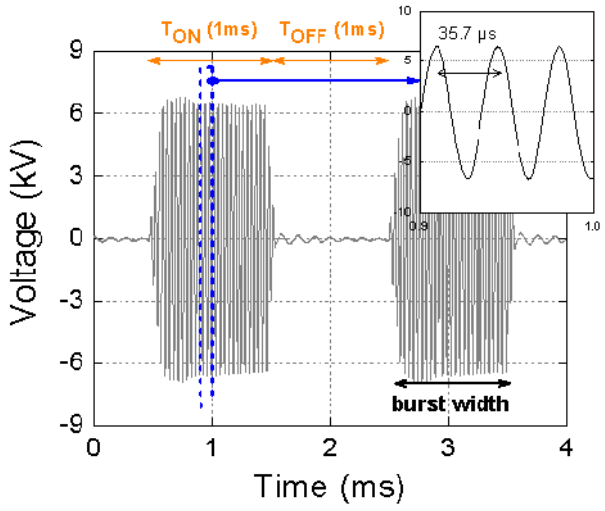

Figure 12: High voltage signals applied to the discharge, with frequency of 28.6 kHz (or period of 35.7 µs) in burst mode with a duty cycle of 50% (T_{ON} = T_{OFF} = 1 ms).

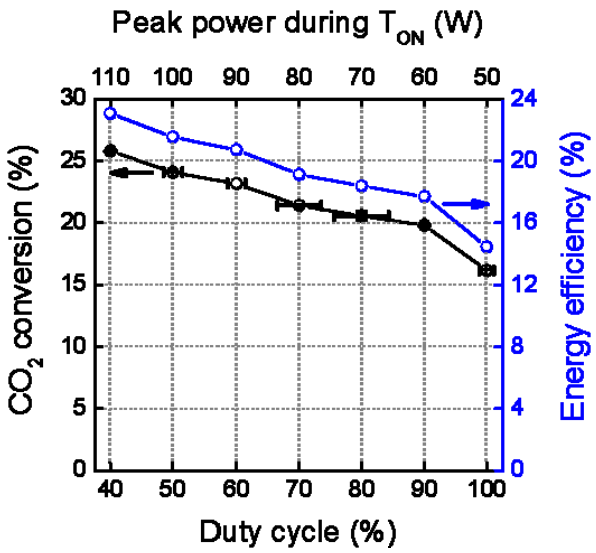

Figure 13: CO_2 conversion and energy efficiency as a function of the duty cycle – $P_{applied}$ = 50 W, f_{signal} = 28.6 kHz, $f_{repetition}$ = 400-900 Hz and $\Phi(CO_2)$ = 200 $mL_n.min^{-1}$.

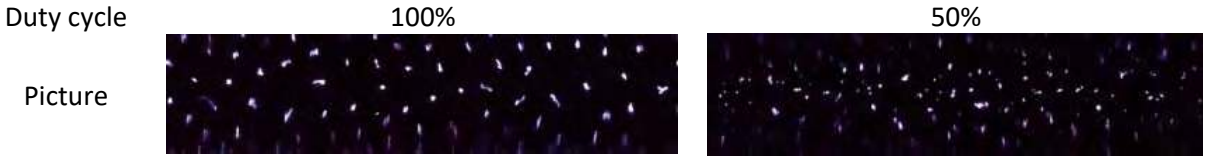

Figure 14: Pictures of the distribution of the microdischarges in the DBD for 100 and 50% duty cycle. $P_{applied}$ = 50 W, f_{signal} = 28.6 kHz and $\Phi(CO_2)$ = 200 $mL_n.min^{-1}$. Camera aperture is 1/100 s.

Concluding remarks

The splitting of CO_2 is an endothermic process, which will always require quite some energy to proceed. A dielectric barrier discharge operating at atmospheric pressure can represent an interesting approach for CO_2 splitting. Indeed, DBD reactors are generally of a simple design, they can easily adapt to industrial gas exhaust systems, and they can be scaled up using simple electrical rules. However, the splitting process is not very efficient, as it proceeds through electronic excitation, and thus it requires a careful approach of the global setup, in order to maximize the conversion and the energy efficiency. The examples listed above show that using a rigorous approach, and with a deep analysis of the DBD behavior, one can significantly increase the conversion. To maximize the conversion, one should ideally have a high density of high energy electrons, one should avoid as much as possible any energy losses, and one should maximize the probability of interaction between the CO_2 molecules and high energy electrons.

Classical approaches consist in increasing the power (to increase the number of electrons), or decreasing the flow rate (to increase the residence time, and therefore to increase the probability of reaction). They are efficient, but one can argue that increasing the power and lowering the flow rates

might not be suitable options for large scale processes, where the aim is to increase the speed at a reasonable energy cost. One can also use non-conventional approaches, which all have a solid scientific explanation. To increase the number of high density electrons while keeping the power low, pulsing the plasma is an interesting approach, as it concentrates the power delivered to the discharge in a very short period of time. This increases the plasma voltage, and therefore the electron energy.

To increase the probability of interaction, CO_2 plasmas being filamentary by nature, we have shown that the number of filaments (microdischarges) is important, as well as their distribution within the whole volume of the discharge. To tune this parameter, the nature and the thickness of the dielectric are very simple parameters to modify, which will not affect the global cost of the reaction itself.

To limit energy losses by heat, leading also to gas expansion, one should keep the gas temperature as low as possible. Therefore, pulsing the power (allowing some time off), and having reactor walls with a good thermal conductivity are possible approaches.

Finally, in Table 3 and Figure 15 we present a summary of the conversion and energy efficiency values obtained in this work, together with some of the main results from the literature. For clarity, the most important operating conditions are also listed in Table 3. As evidenced from Figure 15, our results are comparable or better than the results found in literature, but the main challenge for future possible application is to combine a high conversion with a high energy efficiency. Our proposed approach tries, to some extent, to combine these two features. Especially applying a lower frequency, and/or a pulsed power (so-called burst mode) seem to be very promising in this respect.

Table 3: Comparison of CO_2 conversions obtained in literature for a pure CO_2 plasma ignited via DBD operating at atmospheric pressure ([a] packed bed DBD). The conditions used in the literature are also mentioned.

#	Frequency (kHz)	Power (W)	CO_2 flow rate ($mL.min^{-1}$)	SEI ($eV.molecule^{-1}$)	CO_2 conversion (%)	Energy efficiency (%)	Ref.
1 [a]	9	50	50	15.2	28.5	5.5	[11]
2 [a]	9	20	50	6.1	14.0	6.8	[11]
3 [a]	13.5	35.2	40	13.4	20.4	4.5	[12]
4 [a]	13.5	21.5	40	8.2	16.0	5.7	[12]
5	10-30	20-180	50-600	57.0	50.0	2.6	[49]
6	10-30	20-180	50-600	14.0	25.2	5.3	[49]
7	10-30	20-180	50-600	2.0	7.5	11.1	[49]
8	10	100	50	30.4	24.5	2.4	[14]
9	60	200	50	60.9	30.0	1.4	[14]
10	30	150	200	11.4	13.7	3.5	[14]
11	23.5	17	100	2.6	9.0	10.2	[32]

12	23.5	20	50	6.1	15.0	7.2	[32]
13	23.5	40	25	24.4	29.0	3.5	[32]
14 [a]	23.5	80	20	60.9	42.0	2.0	[50]
15 [a]	23.5	80	50	24.4	24.0	2.9	[50]
16	23.5	100	1000	1.5	2.7	5.2	[51]
17 [a]	5	12	100	1.8	1.6	2.6	[52]
18 [a]	5	6	100	0.9	1.0	3.2	[52]
19	23.5	80	300	4.1	6.0	4.3	[33]
20 → 21	our work: increasing the CO_2 flow rate from 50 to 2000 $mL_n.min^{-1}$						/
22 → 23	our work: decreasing the operating frequency from 28.6 to 16.2 kHz						[15]
24 → 25	our work: increasing the plasma power from 10 to 97 W						[15]
26 → 27 → 28	our work: increasing the barrier thickness from 2 to 2.4 mm and from 2.4 to 2.8 mm						[24]
29 → 30	our work: decreasing the duty cycle from 100 to 50% (from pure AC to burst regime)						[25]

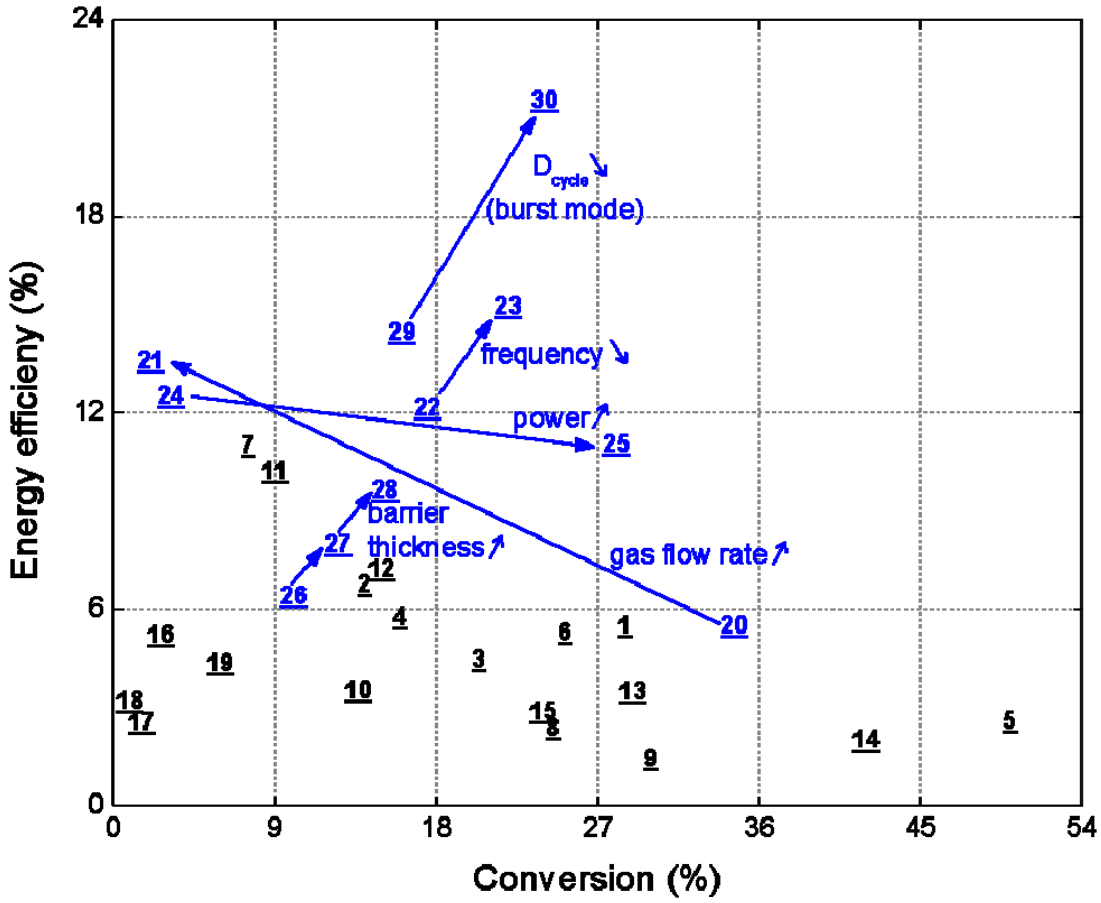

Figure 15: Energy efficiency versus conversion for CO_2 splitting in an atmospheric pressure DBD operating in pure CO_2. The values are taken from the literature (black) as well as from this work (blue) and the blue arrows show the evolution of the conversion/energy efficiency by changing the parameters), and are listed in Table 3.

Other routes, not present in this article, could also be of interest for further improvements of the CO_2 splitting process. It is not directly related to the CO_2 topic but for instance, it is known that an external magnetic field can affect the properties of the plasma [53]. Jiang et al showed that such a magnetic field can improve the size

and the homogeneity of the discharge itself, leading to an entanglement of the microdischarges in a DBD enhanced DC glow discharge at atmospheric pressure.

Acknowledgments

The authors acknowledge financial support from the IAP-VII/12, P7/34 (Interuniversity Attraction Pole) program "PSI-Physical Chemistry of Plasma-Surface Interactions" financially supported by the Belgian Federal Office for Science Policy (BELSPO). A. Ozkan would like to thank the financial support given by the "Fonds David et Alice Van Buuren".

References

[1] A. Grill, *Cold plasma in materials fabrication*: (IEEE Press, New York; 1994).
[2] L. Spencer and A. Gallimore, CO2 dissociation in an atmospheric pressure plasma/catalyst system: a study of efficiency, *Plasma Sources Science and Technology*, **22**(1) (2013) 015019
[3] A. Vesel, M. Mozetic, A. Drenik and M. Balat-Pichelin, Dissociation of CO 2 molecules in microwave plasma, *Chemical Physics*, **382**(1) (2011) 127-131
[4] T. Silva, N. Britun, T. Godfroid and R. Snyders, Optical characterization of a microwave pulsed discharge used for dissociation of CO2, *Plasma Sources Science and Technology*, **23**(2) (2014) 025009
[5] A. Fridman, S. Nester, L.A. Kennedy, A. Saveliev and O. Mutaf-Yardimci, Gliding arc gas discharge, *Progress in Energy and Combustion Science*, **25**(2) (1999) 211-231
[6] T. Nunnally, K. Gutsol, A. Rabinovich, A. Fridman, A. Gutsol and A. Kemoun, Dissociation of CO2 in a low current gliding arc plasmatron, *Journal of Physics D: Applied Physics*, **44**(27) (2011) 274009
[7] A. Indarto, J.-W. Choi, H. Lee and H.K. Song, Conversion of CO2 by gliding arc plasma, *Environmental engineering science*, **23**(6) (2006) 1033-1043
[8] A. Indarto, D.R. Yang, J.-W. Choi, H. Lee and H.K. Song, Gliding arc plasma processing of CO 2 conversion, *Journal of hazardous materials*, **146**(1) (2007) 309-315
[9] F. Brehmer, S. Welzel, M. van de Sanden and R. Engeln, CO and byproduct formation during CO2 reduction in dielectric barrier discharges, *Journal of Applied Physics*, **116**(12) (2014) 123303
[10] X. Duan, Y. Li, W. Ge and B. Wang, Degradation of CO2 through dielectric barrier discharge microplasma, *Greenhouse Gases: Science and Technology*, **5**(2) (2015) 131-140
[11] D. Mei, X. Zhu, Y.-L. He, J.D. Yan and X. Tu, Plasma-assisted conversion of CO2 in a dielectric barrier discharge reactor: understanding the effect of packing materials, *Plasma Sources Science and Technology*, **24**(1) (2015) 015011
[12] Q. Yu, M. Kong, T. Liu, J. Fei and X. Zheng, Characteristics of the decomposition of CO2 in a dielectric packed-bed plasma reactor, *Plasma Chemistry and Plasma Processing*, **32**(1) (2012) 153-163
[13] S. Wang, Y. Zhang, X. Liu and X. Wang, Enhancement of CO2 Conversion Rate and Conversion Efficiency by Homogeneous Discharges, *Plasma Chemistry and Plasma Processing*, **32**(5) (2012) 979-989

[14] S. Paulussen, B. Verheyde, X. Tu, C. De Bie, T. Martens, D. Petrovic, A. Bogaerts and B. Sels, Conversion of carbon dioxide to value-added chemicals in atmospheric pressure dielectric barrier discharges, *Plasma Sources Science and Technology*, **19**(3) (2010) 034015
[15] A. Ozkan, T. Dufour, T. Silva, N. Britun, R. Snyders, A. Bogaerts and F. Reniers, The influence of power and frequency on the filamentary behavior of a flowing DBD—application to the splitting of CO2, *Plasma Sources Science and Technology*, **25**(2) (2016) 025013
[16] A. Ozkan, T. Dufour, G. Arnoult, P. De Keyzer, A. Bogaerts and F. Reniers, CO2–CH4 conversion and syngas formation at atmospheric pressure using a multi-electrode dielectric barrier discharge, *Journal of CO2 utilization*, **9** (2015) 74-81
[17] R. Snoeckx, A. Ozkan, F. Reniers and A. Bogaerts, The quest for value-added products from CO2 and H2O in a dielectric barrier discharge: a chemical kinetics study, *accepted in ChemSusChem*, (2016)
[18] M. Scapinello, L. Martini, G. Dilecce and P. Tosi, Conversion of CH4/CO2 by a nanosecond repetitively pulsed discharge, *Journal of Physics D: Applied Physics*, **49**(7) (2016) 075602
[19] X.S. Li, B. Zhu, C. Shi, Y. Xu and A.M. Zhu, Carbon dioxide reforming of methane in kilohertz spark-discharge plasma at atmospheric pressure, *AIChE Journal*, **57**(10) (2011) 2854-2860
[20] B. Zhu, X.-S. Li, C. Shi, J.-L. Liu, T.-L. Zhao and A.-M. Zhu, Pressurization effect on dry reforming of biogas in kilohertz spark-discharge plasma, *international journal of hydrogen energy*, **37**(6) (2012) 4945-4954
[21] B. Zhu, X.-S. Li, J.-L. Liu, X. Zhu and A.-M. Zhu, Kinetics study on carbon dioxide reforming of methane in kilohertz spark-discharge plasma, *Chemical Engineering Journal*, **264** (2015) 445-452
[22] V. Shapoval, E. Marotta, C. Ceretta, N. Konjević, M. Ivković, M. Schiorlin and C. Paradisi, Development and Testing of a Self-Triggered Spark Reactor for Plasma Driven Dry Reforming of Methane, *Plasma Processes and Polymers*, **11**(8) (2014) 787-797
[23] V. Shapoval and E. Marotta, Investigation on Plasma-Driven Methane Dry Reforming in a Self-Triggered Spark Reactor, *Plasma Processes and Polymers*, **12**(8) (2015) 808-816
[24] A. Ozkan, T. Dufour, A. Bogaerts and F. Reniers, How do the barrier thickness and dielectric material influence the filamentary mode and CO2 conversion in a flowing DBD?, *Plasma Sources Science and Technology*, **25**(4) (2016) 045016
[25] A. Ozkan, T. Dufour, T. Silva, N. Britun, R. Snyders, F. Reniers and A. Bogaerts, DBD in burst mode: solution for more efficient CO2 conversion?, *Plasma Sources Science and Technology*, **25**(5) (2016) 055005
[26] F. Massines, N. Gherardi, N. Naude and P. Segur, Glow and Townsend dielectric barrier discharge in various atmosphere, *Plasma physics and controlled fusion*, **47**(12B) (2005) B577
[27] S. Liu and M. Neiger, Electrical modelling of homogeneous dielectric barrier discharges under an arbitrary excitation voltage, *Journal of Physics D: Applied Physics*, **36**(24) (2003) 3144
[28] S. Liu and M. Neiger, Excitation of dielectric barrier discharges by unipolar submicrosecond square pulses, *Journal of Physics D: Applied Physics*, **34**(11) (2001) 1632
[29] S. Tao, L. Kaihua, Z. Cheng, Y. Ping, Z. Shichang and P. Ruzheng, Experimental study on repetitive unipolar nanosecond-pulse dielectric barrier discharge in air at atmospheric pressure, *Journal of Physics D: Applied Physics*, **41**(21) (2008) 215203
[30] T. Manley, The electric characteristics of the ozonator discharge, *Transactions of the electrochemical society*, **84**(1) (1943) 83-96
[31] H.-E. Wagner, R. Brandenburg, K. Kozlov, A. Sonnenfeld, P. Michel and J. Behnke, The barrier discharge: basic properties and applications to surface treatment, *Vacuum*, **71**(3) (2003) 417-436
[32] R. Aerts, W. Somers and A. Bogaerts, Carbon Dioxide Splitting in a Dielectric Barrier Discharge Plasma: A Combined Experimental and Computational Study, *ChemSusChem*, **8**(4) (2015) 702-716

[33] M. Ramakers, I. Michielsen, R. Aerts, V. Meynen and A. Bogaerts, Effect of argon or helium on the CO2 conversion in a dielectric barrier discharge, *Plasma Processes and Polymers*, **12** (2015) 755-763
[34] X. Tu, H.J. Gallon, M.V. Twigg, P.A. Gorry and J.C. Whitehead, Dry reforming of methane over a Ni/Al2O3 catalyst in a coaxial dielectric barrier discharge reactor, *Journal of Physics D: Applied Physics*, **44**(27) (2011) 274007
[35] H. Jiang, T. Shao, C. Zhang, W. Li, P. Yan and E. Schamiloglu, editors. Study on QV Lissajous figures in nanosecond-pulsed surface discharge. Power Modulator and High Voltage Conference (IPMHVC), 2012 IEEE International; 2012: IEEE.
[36] H. Jiang, T. Shao, C. Zhang, W. Li, P. Yan, X. Che and E. Schamiloglu, Experimental study of QV Lissajous figures in nanosecond-pulse surface discharges, *Dielectrics and Electrical Insulation, IEEE Transactions on*, **20**(4) (2013) 1101-1111
[37] T. Shao, H. Jiang, C. Zhang, P. Yan, M.I. Lomaev and V.F. Tarasenko, Time behaviour of discharge current in case of nanosecond-pulse surface dielectric barrier discharge, *EPL (Europhysics Letters)*, **101**(4) (2013) 45002
[38] R. Valdivia-Barrientos, J. Pacheco-Sotelo, M. Pacheco-Pacheco, J. Benitez-Read and R. López-Callejas, Analysis and electrical modelling of a cylindrical DBD configuration at different operating frequencies, *Plasma sources science and technology*, **15**(2) (2006) 237
[39] U. Kogelschatz, Filamentary, patterned, and diffuse barrier discharges, *Plasma Science, IEEE Transactions on*, **30**(4) (2002) 1400-1408
[40] R. Shrestha, R. Tyata and D. Subedi, Effect of applied voltage in electron density of homogeneous dielectric barrier discharge at atmospherice pressure, *Himalayan Physics*, **4** (2013) 10-13
[41] A.J. Wu, H. Zhang, X.D. Li, S.Y. Lu, C.M. Du and J.H. Yan, Determination of Spectroscopic Temperatures and Electron Density in Rotating Gliding Arc Discharge, *Plasma Science, IEEE Transactions on*, **43**(3) (2015) 836-845
[42] A. Fridman, *Plasma chemistry*: (Cambridge university press; 2008).
[43] T. Kozák and A. Bogaerts, Evaluation of the energy efficiency of CO2 conversion in microwave discharges using a reaction kinetics model, *Plasma Sources Science and Technology*, **24**(1) (2015) 015024
[44] T. Kozàk and A. Bogaerts, Splitting of CO2 by vibrational excitation in non-equilibrium plasmas: A reaction kinetics model, *Plasma Sources Science and Technology*, **23**(4) (2014) 045004
[45] A. Bogaerts, T. Kozàk, K. Van Laer and R. Snoeckx, Plasma-based conversion of CO2: current status and future challenges, *Faraday discussions*, **183** (2015) 217-232
[46] R. Aerts, T. Martens and A. Bogaerts, Influence of vibrational states on CO2 splitting by dielectric barrier discharges, *The Journal of Physical Chemistry C*, **116**(44) (2012) 23257-23273
[47] Y. Akishev, G. Aponin, A. Balakirev, M. Grushin, V. Karalnik, A. Petryakov and N. Trushkin, Role of the volume and surface breakdown in a formation of microdischarges in a steady-state DBD, *The European Physical Journal D*, **61**(2) (2011) 421-429
[48] R. Siliprandi, H. Roman, R. Barni and C. Riccardi, Characterization of the streamer regime in dielectric barrier discharges, *Journal of applied physics*, **104**(6) (2008) 063309
[49] I. Belov, S. Paulussen and A. Bogaerts, Appearance of a conductive carbonaceous coating in a CO2 dielectric barrier discharge and its influence on the electrical properties and the conversion efficiency, *Plasma Sources Science and Technology*, **25**(1) (2016) 015023
[50] K. Van Laer and A. Bogaerts, Improving the Conversion and Energy Efficiency of Carbon Dioxide Splitting in a Zirconia-Packed Dielectric Barrier Discharge Reactor, *Energy Technology*, **3**(10) (2015) 1038-1044
[51] R. Aerts, R. Snoeckx and A. Bogaerts, In-Situ Chemical Trapping of Oxygen in the Splitting of Carbon Dioxide by Plasma, *Plasma Processes and Polymers*, **11**(10) (2014) 985-992
[52] T. Butterworth, R. Elder and R. Allen, Effects of particle size on CO 2 reduction and discharge characteristics in a packed bed plasma reactor, *Chemical Engineering Journal*, **293** (2016) 55-67

[53] W. Jiang, J. Tang, Y. Wang, W. Zhao and Y. Duan, A low-power magnetic-field-assisted plasma jet generated by dielectric-barrier discharge enhanced direct-current glow discharge at atmospheric pressure, *Appl. Phys. Lett.*, **104** (2014) 013505